Chapter 4

CONSERVATION LAWS WITH SOURCE TERMS

It was claimed in Chapter 1 that, in general, a conservation law that is expressed on a manifold has the form (1.4). In the following chapter the details for the derivation of this equation will be presented and the functional form of the source term will be derived. In this chapter, however, we consider the general balance law

$$\boldsymbol{q}_{,t} + \boldsymbol{f}^{(k)}(\boldsymbol{q})_{,k} = \boldsymbol{\psi}(t, \vec{x}, \boldsymbol{q}), \tag{4.1}$$

consisting of a conservation law with a source term that may depend on the components of time, space, and $\boldsymbol{q}$. Balance laws occur in many different applications, conservation laws expressed on manifolds being one example. Other examples also arise for shallow-water flow over varying bottom topography as discussed in [49] and [80]. A treatment of the source terms that appear in the approximation of detonation waves is discussed by Helzel, LeVeque, and Warnecke in [34].

Various methods have been developed for balance laws with an autonomous flux function $f(\boldsymbol{q})$ (e.g. [28], [37], [49], [70]). One common approach, called a split method, is to alternate between solving a homogeneous version of the balance law

$$\boldsymbol{q}_{,t} + \boldsymbol{f}^{(k)}(\boldsymbol{q})_{,k} = 0, \tag{4.2}$$

and the ordinary differential equation

$$\boldsymbol{q}_{,t} = \boldsymbol{\psi}(t, \vec{x}, \boldsymbol{q}). \tag{4.3}$$

Although this approach works well on many problems, there are disadvantages to split methods. For example, the boundary conditions imposed on the split problem should represent the true boundary conditions for the balance law. It may not be a simple task to generate the split boundary conditions. Another disadvantage of split methods is that they do not handle steady solutions very well.

Near steady state, the flux is nearly balanced by the source term so that $|\boldsymbol{q}_{,t}| \ll |\boldsymbol{f}_{,x}| \sim |\boldsymbol{\psi}|$. In order to capture this near-equilibrium flow, the split method must rely on the cancellation of artificially induced dynamics. As an example, consider a fluid in hydrostatic balance so that the flux produced by the pressure is nearly balanced by the gravitational source term. The first step of a split method neglects the flux term, resulting in a large inflow due to the gravitational field. The second step neglects gravity, producing a large outflow due to the pressure forces. Small perturbations on top of this near-steady flow may be lost due to the subtraction of these large and opposite flows. Rather than splitting off the source term in this case, it makes more sense to incorporate it into the Riemann problems that are solved in the homogeneous equation (4.2).

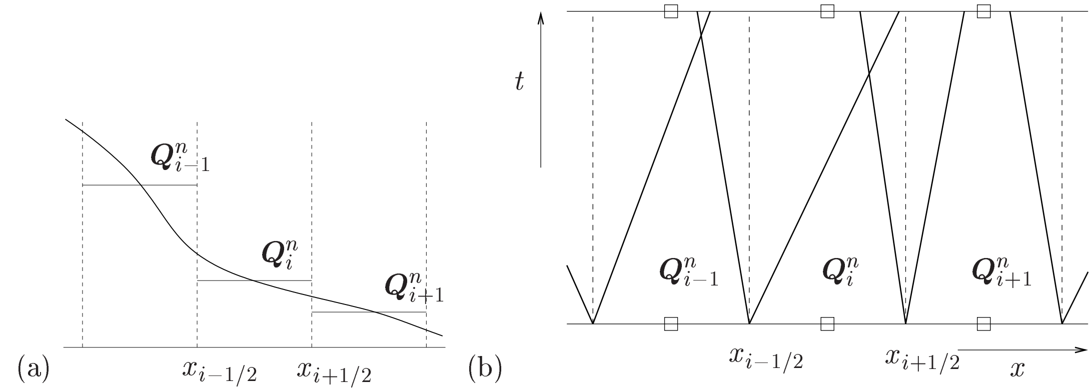

Figure 4.1: (a) Standard cell averaging (b) Wave propagation from cell interfaces resulting from solving the Riemann problems.

Like the previous example, it will be shown in Chapter 6 that it is also natural to incorporate the source terms generated by the geometry of a manifold into Riemann problems. In this chapter, therefore, we study two approaches based on wave propagation, both incorporating source terms into Riemann problems. The first approach, originally developed by LeVeque in [49], is called the quasi-steady wave propagation algorithm. This approach was applied to the Euler equations by LeVeque and Bale in [47]. The original quasi-steady method treats the source using an explicit, one-step method. The presentation here is an extension of this algorithm to multi-step methods. It will be shown that this approach handles near steady solutions very well. However, it will also be shown that this approach is impractical to use in an algorithm that solves general conservation laws on manifolds.

The second approach presented in this chapter incorporates the source term into the flux difference. This modified difference can then be used to generate f-waves as discussed in the previous chapter. This approach is shown to handle near-steady solutions very well. In addition, it does not share some of the disadvantages of the quasi-steady method, making it useful for the main goal of this dissertation; developing an algorithm for the solution of conservation laws on manifolds.

4.1 Multi-step Quasi-Steady Wave Propagation

Let us begin by studying the multi-step quasi-steady wave propagation method. As for the wave propagation methods developed in Chapter 2, one-dimensional data on each time slice is represented by piecewise constant functions having cell centered values $\boldsymbol{Q}_i^n$ at the n^{th} time level and in the i^{th} cell denoted by $\mathcal{C}_i \equiv [x_{i-1/2}, x_{i-1/2} + \Delta x]$. This finite volume representation of a function is depicted in Figure 4.1(a). The standard wave propagation algorithm, developed by LeVeque in [45], and reviewed in Section 2.3, is implemented in the software package CLAWPACK for the solution of homogeneous conservation laws like (4.2). If a source term exists, CLAWPACK provides routines to implement a split method

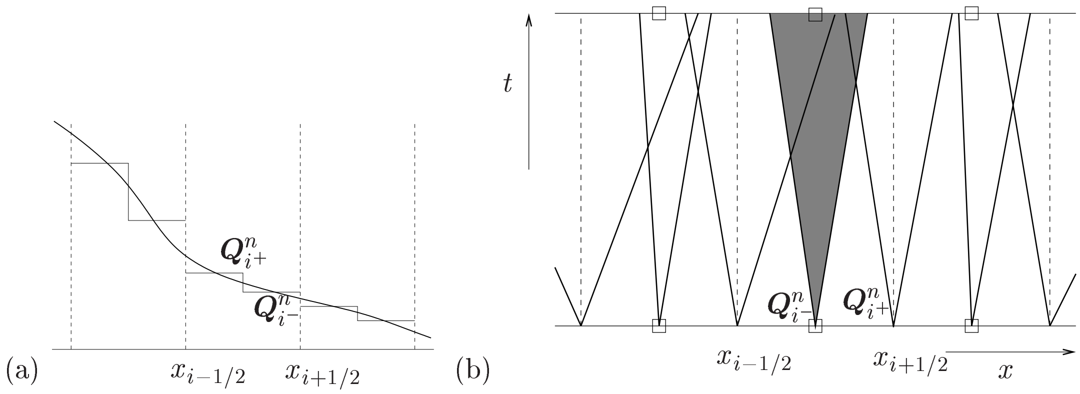

Figure 4.2: (a) Modified cell averages for the quasi-steady approach. (b) Wave propagation with cell centered Riemann problems included.

such as Strang or Godunov splitting. Suppose, instead, that it is beneficial to incorporate the source term into the Riemann problems. The quasi-steady wave propagation algorithm accomplishes this by introducing a jump in the center of each cell as depicted in Figure 4.2(a). The jump in the i^{th} cell has magnitude $|\boldsymbol{Q}^n_{i+} - \boldsymbol{Q}^n_{i-}|$ where the quantities $\boldsymbol{Q}^n_{i-}$ and $\boldsymbol{Q}^n_{i+}$ are defined in the left and right half of that cell, respectively. The jump at the center of the i^{th} cell is chosen such that the following conditions are satisfied:

$$\frac{1}{2}\left(\boldsymbol{Q}^n_{i-} + \boldsymbol{Q}^n_{i+}\right) = \boldsymbol{Q}^n_i \tag{4.4}$$

$$\boldsymbol{f}(\boldsymbol{Q}^n_{i+}) - \boldsymbol{f}(\boldsymbol{Q}^n_{i-}) = \Delta x \sum_{k=0}^{M-1} \alpha_k \boldsymbol{\psi}^{n-k}_i, \tag{4.5}$$

where we define $\boldsymbol{\psi}^n_i = \boldsymbol{\psi}(t^n, x_i, \boldsymbol{Q}^n_i)$. The first condition assures that the method will remain conservative by leaving cell averages unchanged. The second, as will be demonstrated below, assures that the cell is updated in such a way that the waves emanating from the cell-centered Riemann problems exactly cancel the influence of the source.

If the Courant number is chosen to be less than 1/2 (this restriction is only temporary) on each time slice, then waves generated by the jump located at the center of the i^{th} cell will remain entirely within the i^{th} cell. The domain of influence of the Riemann problem at the center of the i^{th} cell for such Courant numbers is depicted by the shaded region of Figure 4.2(b). Since these cell centered Riemann problems do not influence neighboring cells, it is unnecessary to resolve the resulting flux difference $\boldsymbol{f}(\boldsymbol{Q}^n_{i+}) - \boldsymbol{f}(\boldsymbol{Q}^n_{i-})$ into right and left going pieces. Rather, this entire flux difference is added into the update for $\boldsymbol{Q}^{n+1}_i$. We must also consider the influence of the source. The influence of the source over a time step is included according to the explicit M-step method

$$\boldsymbol{Q}^{n+1}_i = \boldsymbol{Q}^n_i + \Delta t \left(\sum_{k=0}^{M-1} \alpha_k \boldsymbol{\psi}^{n-k}_i \right). \tag{4.6}$$

The set of coefficients $\{\alpha_0, \cdots, \alpha_{M-1}\}$ are the standard Adams-Bashforth multi-step coefficients. As for the standard algorithm, the influence of incoming waves at the right and left edge of the i^{th} cell is denoted by the fluctuations $\boldsymbol{\mathcal{A}}^{+}\boldsymbol{\Delta Q}_{i-1/2}$ and $\boldsymbol{\mathcal{A}}^{-}\boldsymbol{\Delta Q}_{i+1/2}$, respectively. The unsplit modified update that incorporates the fluctuations and the influence of the source (4.6) can be written

$$\begin{aligned} \boldsymbol{Q}_i^{n+1} = \boldsymbol{Q}_i^n &- \frac{\Delta t}{\Delta x}\left(\boldsymbol{\mathcal{A}}^{+}\boldsymbol{\Delta}\tilde{\boldsymbol{Q}}_{i-1/2} - \boldsymbol{\mathcal{A}}^{-}\boldsymbol{\Delta}\tilde{\boldsymbol{Q}}_{i+1/2}\right) \\ &+ \Delta t\left[\sum_{k=0}^{M-1}\alpha_k\boldsymbol{\psi}_i^{n-k} - \frac{1}{\Delta x}\left(\boldsymbol{f}(\boldsymbol{Q}_{i^+}^n) - \boldsymbol{f}(\boldsymbol{Q}_{i^-}^n)\right)\right]. \end{aligned} \tag{4.7}$$

The tildes on $\boldsymbol{\mathcal{A}}^{+}\boldsymbol{\Delta}\tilde{\boldsymbol{Q}}_{i-1/2}$ and $\boldsymbol{\mathcal{A}}^{-}\boldsymbol{\Delta}\tilde{\boldsymbol{Q}}_{i+1/2}$ serve as a reminder that the waves generated in Riemann problems are now based on modified data $\boldsymbol{Q}_{i-1^+}^n$ and $\boldsymbol{Q}_{i^-}^n$.

This update is a multi-step generalization of the quasi-steady updates used in [49] and [47]. The influence of the source in equation (4.7) is handled in a more accurate way for $M > 1$. It should be noted that this generalization includes the original quasi-steady update for $M = 1$.

If equation (4.5) is satisfied, then the terms in square brackets drop out completely and the first order update reduces to

$$\boldsymbol{Q}_i^{n+1} = \boldsymbol{Q}_i^n - \frac{\Delta t}{\Delta x}\left(\boldsymbol{\mathcal{A}}^{+}\boldsymbol{\Delta}\tilde{\boldsymbol{Q}}_{i-1/2} + \boldsymbol{\mathcal{A}}^{-}\boldsymbol{\Delta}\tilde{\boldsymbol{Q}}_{i+1/2}\right), \tag{4.8}$$

which looks identical to the update (2.31), but with fluctuations $\boldsymbol{\mathcal{A}}^{\pm}\boldsymbol{\Delta}\tilde{\boldsymbol{Q}}_{i-1/2}$ determined by solving the Riemann problems with data $\boldsymbol{Q}_{i-1^+}^n$ and $\boldsymbol{Q}_{i^-}^n$, as depicted in Figure 4.2(a), rather than the original flux-difference $\boldsymbol{\mathcal{A}}^{\pm}\boldsymbol{\Delta Q}_{i-1/2}$ based on $\boldsymbol{Q}_{i-1}^n$ and $\boldsymbol{Q}_i^n$ of Figure 4.1(a).

A natural choice for the shifted data in each cell is

$$\boldsymbol{Q}_{i^\pm}^n = \boldsymbol{Q}_i^n \pm \boldsymbol{\delta}_i, \tag{4.9}$$

so that equation (4.4) is satisfied identically. Using $\boldsymbol{\delta}_i$, we can rewrite equation (4.5) as

$$\begin{aligned} \boldsymbol{f}(\boldsymbol{Q}_i^n + \boldsymbol{\delta}_i) - \boldsymbol{f}(\boldsymbol{Q}_i^n - \boldsymbol{\delta}_i) &= \Delta x\sum_{k=0}^{M-1}\alpha_k\boldsymbol{\psi}_i^{n-k} \\ &= \Delta x\,\boldsymbol{\Theta}^M, \end{aligned} \tag{4.10}$$

where we have introduced the vector $\boldsymbol{\Theta}^M$ with a superscript denoting its dependence on the multi-step parameter M. The components of $\boldsymbol{\Theta}^M$ have absorbed the sum that appears on the right side of the first equality in the previous equation. If we denote the K^{th} component of the vectors $\boldsymbol{\psi}_i^n$ and $\boldsymbol{\Theta}^M$ by $\psi_{i[K]}^n$ and $\Theta_{[K]}^M$, respectively, then the components of $\boldsymbol{\Theta}^M$ are defined to be

$$\Theta_{[K]}^M = \begin{cases} \psi_{i[K]}^n\left(\alpha_0 + \sum_{k=1}^{M-1}\alpha_k\frac{\psi_{i[K]}^{n-k}}{\psi_{i[K]}^n}\right) & \text{if } \psi_{i[K]}^n \neq 0 \text{ for each } K \\ \psi_{i[K]}^n & \text{if } \psi_{i[K]}^n = 0 \text{ for any } K. \end{cases} \tag{4.11}$$

Note that if $M = 1$, then we are using the one-step Adams-Bashforth method (Euler's method) with $\alpha_0 = 1$. In this case equation (4.10) reduces to the original condition reported in [49] and [47].

Equation (4.10) is an algebraic system that must be solved for the components of the $\boldsymbol{\delta}_i$ that tell us how to modify the Riemann data. For $M > 1$ the components of the vector $\boldsymbol{\Theta}^M$ change the solution of this system to improve accuracy. Once equation (4.10) is solved, state variables are shifted according to equation (4.9) and Riemann problems based on $\boldsymbol{Q}^n_{i\pm}$ are solved. In fact, the shifted data is that which arises from the dynamical perturbations in the quasi-steady state. For this reason, the quasi-steady wave propagation method accurately captures quasi-steady solutions.

Although we derived this method assuming the Courant number is less than 1/2, the resulting method is stable for Courant numbers up to 1 due to the fact that the waves emanating from cell-centered Riemann problems are eliminated completely.

4.1.1 High resolution corrections and CLAWPACK*implementation*

The modified Riemann problem between states $\boldsymbol{Q}^n_{i-1^+}$ and $\boldsymbol{Q}^n_{i^-}$ gives rise to a set of waves $\mathcal{W}^p_{i-1/2}$ for $p = 1, \cdots, M_w$ with associated speeds $\lambda^p_{i-1/2}$ such that

$$\Delta \boldsymbol{Q}^n_i \equiv \boldsymbol{Q}^n_{i^-} - \boldsymbol{Q}^n_{i-1^+} = \sum_{p=1}^{M_w} \boldsymbol{\mathcal{W}}^{(p)}_{i-1/2}. \tag{4.12}$$

The first order method described above is extended to a high resolution method by adding corrections to the update (4.8). A correction flux similar to (2.41) is defined as

$$\tilde{\boldsymbol{F}}_{i-1/2} = \frac{1}{2} \sum_{p=1}^{M_w} |\lambda^p_i| \left(1 - \frac{\Delta t}{\Delta x} |\lambda^p_i|\right) \tilde{\boldsymbol{\mathcal{W}}}^{(p)}_{i-1/2}, \tag{4.13}$$

where the waves in this correction flux are based on the modified data. Once again, the tilde over the wave denotes that it has been limited as described in equation (2.42). Many more details about limiting can be found in [42], [43], and [46]. Incorporating these correction fluxes, the update (4.8) becomes

$$\begin{aligned} \boldsymbol{Q}^{n+1}_i = \boldsymbol{Q}^n_i &- \frac{\Delta t}{\Delta x}\left(\boldsymbol{\mathcal{A}}^+ \boldsymbol{\Delta} \tilde{\boldsymbol{Q}}_{i-1/2} + \boldsymbol{\mathcal{A}}^- \boldsymbol{\Delta} \tilde{\boldsymbol{Q}}_{i+1/2}\right) \\ &- \frac{\Delta t}{\Delta x}\left(\tilde{\boldsymbol{F}}_{i+1/2} - \tilde{\boldsymbol{F}}_{i-1/2}\right). \end{aligned} \tag{4.14}$$

This update looks very similar to the original wave propagation update (2.44), but is based on the modified data.

We implement the algorithm described here in the software package CLAWPACK. Only the Riemann solvers need to be modified. The process of preparing to solve Riemann problems based on the modified data is as follows:

1. Solve equation (4.10) for components of the vector $\boldsymbol{\delta}_i$ in each cell.

2. Modify the states according to equation (4.9).

3. Set up data for the i^{th} Riemann problem by setting the left state to $\boldsymbol{Q}^n_{i-1^+}$, and the right state to $\boldsymbol{Q}^n_{i^-}$.

Once this data has been set up, Riemann problems are solved generating the waves. The limiters are applied only to the waves representing disturbances from the steady state, not to the variations in the steady state itself. This leads to excellent resolution of small dynamic perturbations.

4.1.2 An implementation for the Euler equations

In Sections 4.3 and 4.4 of this chapter, the performance of both the quasi-steady algorithm and the approach presented in Section 4.2 is analyzed by solving the Euler equations for a fluid flowing under the influence of a gravitational force. In order to implement the quasi-steady algorithm on this set of equations, equation (4.10) must be solved. In this section the details of this solution are presented. These results were first presented in [47], but some of those formulas have errors. These errors have been corrected for the formulas presented in this chapter. In Sections 4.3 and 4.4, these results are used in the examples.

The Euler equations express the conservation of mass, momentum, and energy for a fluid. In Appendix B, they are derived for a perfect fluid under the influence of a general body force. The result, with gravity playing the role of the body force, can be written

$$\rho_{,t} + \vec{\nabla} \cdot \rho\vec{u} = 0, \tag{4.15}$$

$$(\rho\vec{u})_{,t} + \vec{\nabla} \cdot (\rho\vec{u} \otimes \vec{u} + \mathbb{I}\, p) = -\rho\vec{\nabla}\phi, \tag{4.16}$$

$$e_{,t} + \vec{\nabla} \cdot [(e+p)\,\vec{u}] = -\rho\vec{u} \cdot \vec{\nabla}\phi, \tag{4.17}$$

where ϕ is the gravitational potential, ρ the fluid density, $\vec{u}$ the velocity, e the fluid energy, and p the pressure. In equation (4.17), e represents the total fluid energy and does not include gravitational potential. This system is closed with the equation of state for a perfect fluid $p = (\gamma - 1)\rho\epsilon$, where ϵ is the specific internal energy. For a given potential ϕ, the gravitational acceleration is defined to be $\vec{a} = -\vec{\nabla}\phi$. It should be noted that the examples presented in this chapter involve a gravitational potential, but the methods presented here will work for any potential giving rise to a force on the fluid.

Wave propagation methods are based solving one-dimensional Riemann problems, so we will consider the Euler equations above along the x-axis. These one-dimensional equations take the form

$$\rho_{,t} + (\rho u)_{,x} = 0, \tag{4.18}$$

$$(\rho u)_{,t} + \left(\rho u^2 + p\right)_{,x} = \rho a^x, \tag{4.19}$$

$$e_{,t} + [(e+p)\,u]_{,x} = \rho u a^x, \tag{4.20}$$

where $\vec{u} = (u, 0, 0)^T$, and a^x is the component of the gravitational acceleration in the x direction. Note that we hesitate to write $a^x = -g$ because we would like to emphasize that we allow dynamic, non-uniform gravitational fields.

At each time step we would like to find components of $\boldsymbol{\delta}_i$ such that equation (4.5) is satisfied. The subscript i denoting quantities in the i^{th} cell will now be dropped and it will be understood that, for example, ρ^n represents the density in the grid cell under consideration at the n^{th} time step. Define $s \equiv \rho u$ and notice that the right hand side of equation (4.18) is zero. To satisfy equation (4.5), equations (4.18)-(4.20) require that

$$s_+^n = s_-^n \equiv s^n, \tag{4.21}$$

$$(\gamma - 1)\left[e_+^n - e_-^n\right] + \frac{(3-\gamma)\,(s^n)^2}{2}\left[\frac{1}{\rho_+^n} - \frac{1}{\rho_-^n}\right] = \Delta x \rho^n a_x^n \Theta_{[s]}, \tag{4.22}$$

$$\gamma s^n \left[\frac{e_+^n}{\rho_+^n} - \frac{e_-^n}{\rho_-^n}\right] - \frac{(\gamma-1)\,(s^n)^3}{2}\left[\left(\frac{1}{\rho_+^n}\right)^2 - \left(\frac{1}{\rho_-^n}\right)^2\right] = \Delta x s^n a_x^n \Theta_{[e]}, \tag{4.23}$$

where we have used $p_\pm^n = \left(\gamma - 1\right)(e_\pm^n - (s^n)^2/2\rho_\pm^n\right)$ to eliminate the pressure and used definition (4.11) to write the components of $\boldsymbol{\Theta}^M$ as

$$\boldsymbol{\Theta}_M = \left(\begin{array}{c}\Theta_{[\rho]}\\ \Theta_{[s]}\\ \Theta_{[e]}\end{array}\right) = \alpha_0 + \sum_{k=1}^{M-1}\alpha_k\left(\begin{array}{c}0\\ \rho^{n-k}(a^x)^{n-k}/\rho^n(a^x)^n\\ s^{n-k}(a^x)^{n-k}/s^n(a^x)^n\end{array}\right), \tag{4.24}$$

when the momentum does not vanish. If it does vanish, then $\boldsymbol{\Theta}^M = (1,1,1)^T$.

The cell centered jump is introduced by defining

$$\rho_\pm^n = \rho^n \pm \tilde{\delta}_\rho \equiv \rho^n \;\left(1 \pm \delta_\rho\right) \tag{4.25}$$

$$e_\pm^n = e^n \pm \tilde{\delta}_e \equiv e^n \;\left(1 \pm \delta_e\right), \tag{4.26}$$

in which physical states must have $\delta_\rho, \delta_e \in (-1,1)$. In terms of δ_ρ and δ_e the non-trivial equations can be written

$$\frac{(s^n)^2(\gamma-3)}{\rho^n}\delta_\rho + \left[2(\gamma-1)e^n\delta_e - \Delta x \rho^n (a^x)^n \Theta_s\right]\left(1-\delta_\rho^2\right) = 0, \tag{4.27}$$

$$s^n\left\{2\left(\frac{s^n}{\rho^n}\right)(\gamma-1)\delta_\rho + \left[\frac{2\gamma e^n}{\rho^n}\left(\delta_e - \delta_\rho\right) - \Delta x \Theta_e\left(1-\delta_\rho^2\right)\right]\left(1-\delta_\rho^2\right)\right\} = 0. \tag{4.28}$$

Using the fact that equation (4.27) is linear in δ_e, this system can be rewritten in the form

$$\delta_e = \mathcal{K}\left(\frac{3-\gamma}{\gamma-1}\right)\frac{\delta_\rho}{1-\delta_\rho^2} + \frac{\mathcal{G}\Theta_s}{2(\gamma-1)}, \tag{4.29}$$

$$\left(\delta_\rho^2 - 1\right)\left[\left(\delta_\rho^2-1\right)\frac{\mathcal{G}\Theta_e}{2\gamma} - \delta_\rho + \frac{\mathcal{G}\Theta_s}{2(\gamma-1)}\right] - \mathcal{K}\frac{\Gamma}{\gamma}\delta_\rho = 0, \tag{4.30}$$

where we have defined the non-dimensional parameters

$$\Gamma \equiv \frac{\gamma^2 - \gamma + 2}{\gamma - 1}, \quad \mathcal{G} \equiv \frac{\Delta x \rho^n (a^x)^n}{e^n}, \quad \mathcal{K} \equiv \frac{(s^n)^2}{2\rho^n e^n}. \tag{4.31}$$

The first parameter, Γ, is nondimensional since γ itself is nondimensional. The parameters $\mathcal{G}$ and $\mathcal{K}$ represent ratios of energies. The parameter $\mathcal{G}$ is the ratio of the difference of gravitational potential energy from cell edge to cell edge to the total fluid energy in that cell. The parameter $\mathcal{K}$ represents the ratio of kinetic to total fluid energy in the cell. The procedure for obtaining both density and energy shifts will be to solve equation (4.30) for δ_ρ, and use this in equation (4.29) to find δ_e.

For quasi-steady flows with length scales determined by L, the gravitational energy density should roughly balance the total fluid energy density. This means that

$$0 < |N \Delta x \rho a^x| \sim e \tag{4.32}$$

on a grid with N cells and $L \sim N\Delta x$. This requires that

$$0 < |\mathcal{G}| \ll 1, \tag{4.33}$$

since $1/N \ll 1$ for a sufficiently refined grid. The last equation implies that equation (4.30) is a fourth order polynomial for δ_ρ with the small parameter $\mathcal{G}$ in front of the highest order term. This singularly perturbed algebraic equation will have one root that behaves as $\mathcal{O}(1/\mathcal{G})$ and will, therefore, be outside of the physically acceptable interval $(-1, 1)$. We seek the physical root by expanding the solutions in an asymptotic power series of $\mathcal{G}$. This expansion can be made easier if we note that given a solution, $\boldsymbol{\delta}(\boldsymbol{q}; \mathcal{G})$, of equations 4.27-4.28 for an acceleration a^x, it must be true that

$$-\boldsymbol{\delta}(\boldsymbol{q}; -\mathcal{G}) = \boldsymbol{\delta}(\boldsymbol{q}; \mathcal{G}) \tag{4.34}$$

is also a solution for a gravitational acceleration of the same magnitude, but in the opposite direction ($a^x \to -a^x$). We can, therefore, seek asymptotic solutions in odd powers of $\mathcal{G}$ of the form

$$\delta_e = \delta_e^1 \mathcal{G} + \delta_e^3 \mathcal{G}^3 + \mathcal{O}(\mathcal{G}^5), \tag{4.35}$$

$$\delta_\rho = \delta_\rho^1 \mathcal{G} + \delta_\rho^3 \mathcal{G}^3 + \mathcal{O}(\mathcal{G}^5). \tag{4.36}$$

Any even powers of $\mathcal{G}$ would destroy the property (4.34).

The expansion for δ_ρ has been computed through $\mathcal{O}(\mathcal{G}^3)$ and can be written as

$$\begin{aligned}\delta_\rho =& \frac{\gamma\Theta_s - (\gamma-1)\,\Theta_e}{2\,(\gamma-1)\,(\gamma-\mathcal{K}\Gamma)}\mathcal{G} + \\ & \frac{\gamma\,(\gamma\Theta_s - (\gamma-1)\,\Theta_e)^2}{8\,(\gamma-1)^2\,(\gamma-\mathcal{K}\Gamma)^4}\left[\left(1 - 2\frac{\mathcal{K}\Gamma}{\gamma}\right)\Theta_e + \frac{\mathcal{K}\Gamma}{\gamma-1}\Theta_s\right]\mathcal{G}^3 + \mathcal{O}(\mathcal{G}^5),\end{aligned} \tag{4.37}$$

corresponding to the energy shift

$$\begin{aligned}\delta_e =& \left[\frac{\Theta_s}{2\,(\gamma-1)} + \frac{\mathcal{K}\,(3-\gamma)\,(\gamma\Theta_s - (\gamma-1)\Theta_e)}{2\,(\gamma-1)^2\,(\gamma-\mathcal{K}\Gamma)}\right]\mathcal{G} + \\ & \frac{\gamma^2\,(\gamma\Theta_s - (\gamma-1)\,\Theta_e)^2}{8\,(\gamma-1)^2\,(\gamma-\mathcal{K})^4}\left[\frac{1}{\gamma-1}\Theta_s - \frac{\mathcal{K}\Gamma}{\gamma^2}\Theta_e\right]\mathcal{G}^3 + \mathcal{O}(\mathcal{G}^5).\end{aligned} \tag{4.38}$$

Figures 4.3(a) and 4.3(b) show these solutions at various orders for a typical grid cell. The

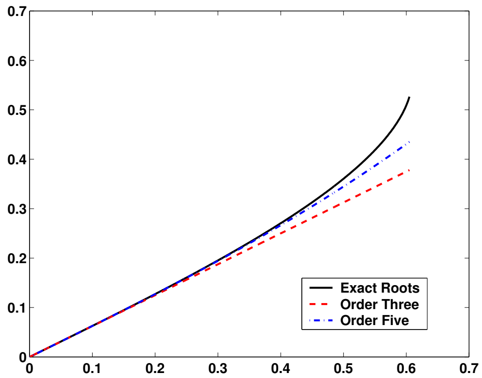

(a) δ_ρ: the density shift

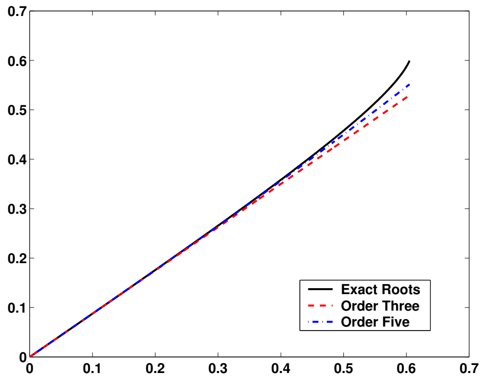

(b) δ_e: the energy shift

Figure 4.3: A comparison of both third and fifth order asymptotics with the exact roots for (a) δ_ρ and (b) δ_e. The finite volume cell is taken to have $\mathcal{K} = 1/10$, $\gamma = 5/3$, $a^x = 1$, and $\mathcal{G} \in [0, 6/10]$. The solid line represents the exact roots as a function of $\mathcal{G}$, the dashed line is an $\mathcal{O}(\mathcal{G}^3)$ asymptotic approximation to these roots, and the dot-dashed line represents an $\mathcal{O}(\mathcal{G}^5)$ approximation.

solid line represents the numerical-exact solution, the dashed line shows that the $\mathcal{O}(\mathcal{G}^3)$ solution does very well for a while. Finally, the figures show that the $\mathcal{O}(\mathcal{G}^5)$ solution remains closer to the exact solution for larger $\mathcal{G}$.

The asymptotic shift solutions computed here can be used directly, or equation (4.37) can be used as an initial guess for an iteration procedure for equation (4.30). This iteration can be carried out to any given tolerance. A Newton iteration was used for the solution represented by solid lines in figures above. Once δ_ρ is known, equation (4.29) is used to find δ_e. Notice that an initial guess of zero fluid momentum is unnecessary for such an iterative process. If we use a one-step method ($M = 1$), then $\Theta_{[e]} = \Theta_{[s]} = 1$ and to first order these expressions for δ_ρ and δ_e reduce to equations (16) and (17) of [47], respectively. In the examples that follow, these shift solutions are used to modify the states.

4.2 A method based on modified flux differences

The quasi-steady method developed in the previous section is not a viable approach for the source terms generated by the geometry of manifolds. The disadvantages suffered by the method include the following:

1. The solution of the system (4.10) to find the amount by which states are modified is different for each system the method is applied to. Nonlinear fluxes have systems that, if a solution exists, are expensive to compute. We have seen this for the Euler equations.

2. If no solution to (4.10) exists, one is forced to return to a split method. This occurs for the Euler equations when momenta become only slightly larger than the steady value.

3. The quasi-steady waves do not naturally fit into the application of f-waves for spatially-varying flux functions.

Therefore, the quasi-steady method is appropriate for solving systems near a steady state, but is not a good choice for problems that are very dynamic. This is too restrictive for the goals of the algorithm developed in this dissertation.

However, the f-wave decomposition discussed in the previous chapter suggests a method that turns out to suffer none of the disadvantages described above. In this approach, the source term $\boldsymbol{\psi}$, is replaced by a function, $\Psi(\boldsymbol{q}, x)$, that consists of delta sources at each interface. This source function, therefore, has the form

$$\boldsymbol{\Psi}(\boldsymbol{q}, x) = \Delta x \sum_{i} \boldsymbol{\Psi}_{i-1/2}\, \delta(x - x_{i-1/2}), \tag{4.39}$$

so that $\boldsymbol{\Psi}$ represents the vector of source values at the interface where $x = x_{i-1/2}$. The source can be incorporated into Riemann problems by modifying equation (3.2) to include the influence of the source,

$$\boldsymbol{q}_{,t} + \mathcal{F}_{i-1/2}(\boldsymbol{q})_{,x} = \Delta x\, \boldsymbol{\Psi}_{i-1/2}\, \delta x - x_{i-1/2}, \tag{4.40}$$

with $\mathcal{F}_{i-1/2}$ given by (3.3) and solving it with the same initial data (2.9). The flux is no longer continuous across the interface due to the delta-function source located there,

$$\boldsymbol{f}_i(\boldsymbol{Q}_i) - \boldsymbol{f}_{i-1}(\boldsymbol{Q}_{i-1}) = \Delta x\, \boldsymbol{\Psi}_{i-1/2}. \tag{4.41}$$

This modified difference suggests that we define the f-waves based on the difference

$$\boldsymbol{f}_i(\boldsymbol{Q}_i) - \boldsymbol{f}_{i-1}(\boldsymbol{Q}_{i-1}) - \Delta x\, \boldsymbol{\Psi}_{i-1/2} = \sum_{p=1}^{n_{eq}} \boldsymbol{\mathcal{Z}}^p_{i-1/2}, \tag{4.42}$$

instead of (3.12).

The approach can be summarized as:

step 1: Define the function $\boldsymbol{\Psi}(\boldsymbol{q}, x)$ so that the $\boldsymbol{\Psi}_{i-1/2}$ is known at each cell interface.

step 2: Decompose the modified flux difference (4.41) into f-waves as shown in (4.42).

step 3: Use the resulting f-waves in the update (3.26) as described in the previous chapter.

The implementation of this approach is much simpler than that for the quasi-steady method and is very natural to apply for systems with spatially-varying flux functions. Though f-waves are used to incorporate the source into Riemann problems, it is not necessary that the flux have spatial variation. An example of this method applied to an autonomous flux is presented in the following two sections.

Notice that there is no restriction on the application of this approach away from steady solutions as there is for the quasi-steady method. However, near steady solutions it is expected that flux gradients balance source terms so that

$$\frac{\boldsymbol{f}_i(\boldsymbol{Q}_i) - \boldsymbol{f}_{i-1}(\boldsymbol{Q}_{i-1})}{\Delta x} \approx \boldsymbol{\Psi}_{i-1/2}. \tag{4.43}$$

In this case, equation (4.41) is nearly satisfied leaving only a small difference on the left side of (4.42) to generate f-waves. Therefore, steady solutions and small perturbations of them are accurately captured by this modified flux difference approach. Examples of this will be seen in the following sections.

4.2.1 Accuracy of the modified flux method

It was demonstrated in Section 3.3 that the wave propagation method based on f-waves is second order provided that $\boldsymbol{q}$ and $\boldsymbol{f}$ remain smooth. This analysis performed there can be repeated taking into consideration the source $\boldsymbol{\psi}$. The Taylor series (3.34) becomes

$$\begin{aligned} \boldsymbol{q}(t_{n+1}, x_i) = \boldsymbol{q}(t,x)|_{t_n,x_i} &- \Delta t\left(\boldsymbol{f}(\boldsymbol{q},x)_{,x} - \boldsymbol{\psi}(\boldsymbol{q},x)\right)|_{t_n,x_i} \\ &+ \frac{1}{2}\Delta t^2 \left[\partial \boldsymbol{f}/\partial \boldsymbol{q}\,(q,x)\left(\boldsymbol{f}(\boldsymbol{q},x)_{,x} - \boldsymbol{\psi}(\boldsymbol{q},x)\right)\right]_{,x}|_{t_n,x_i} \\ &- \partial \boldsymbol{\psi}/\partial \boldsymbol{q}(\boldsymbol{q},x)\left(\boldsymbol{f}(\boldsymbol{q},x)_{,x} - \boldsymbol{\psi}(\boldsymbol{q},x)\right)|_{t_n,x_i} + \mathcal{O}(\Delta t^3). \end{aligned} \tag{4.44}$$

The update (3.26) based on the f-waves defined in (4.42) captures all terms in the Taylor series to second order, except the last term. To make the method fully second order accurate, a term of the form

$$-\frac{\Delta t^2}{2\Delta x}\,\partial \boldsymbol{\psi}/\partial \boldsymbol{q}(\boldsymbol{Q}_i, x_i)\sum_{p=1}^{n_{eq}} \frac{1}{2}\left(\boldsymbol{\mathcal{Z}}^p_{i-1/2} + \boldsymbol{\mathcal{Z}}^p_{i+1/2}\right) \tag{4.45}$$

is added to the right side of the update (3.26).

4.3 An isothermal equilibrium

As an example of both methods described in this chapter, consider an isothermal equilibrium in one space dimension of the form

$$p_0(y) = \alpha\rho_0 = \exp\left[-g(y-y_0)\alpha\right], \tag{4.46}$$
$$u_0(y) = 0, \tag{4.47}$$
$$-\partial_y \phi_0(y) = g, \tag{4.48}$$

on the interval $y \in [0, 3/2]$ and with g constant and $\alpha = 1$. The grid is initialized to this equilibrium and the flow is then evolved.

Table 4.1: One-norm errors for the numerical solutions generated by three methods for the isothermal equilibrium. The method based on Strang splitting only computes the steady solution to first order. The methods based on the multi-step quasi-steady approximation and the modified flux difference both compute second order solutions.

	Strang Splitting	Quasi-Steady ($M = 2$)	Modified Flux Difference
dx	$\|p - p_0\|_1$	$\|p - p_0\|_1$	$\|p - p_0\|_1$
1.500×10^{-2}	5.541×10^{-4}	9.561×10^{-7}	1.602×10^{-6}
7.500×10^{-3}	2.771×10^{-4}	2.365×10^{-7}	3.992×10^{-7}
3.750×10^{-3}	1.388×10^{-4}	5.880×10^{-8}	9.954×10^{-8}
1.875×10^{-3}	6.963×10^{-5}	1.466×10^{-8}	2.485×10^{-8}
order	1.00	2.01	2.00

Table 4.2: One-norm errors for the numerical solutions generated by the same three methods for the perturbed isothermal equilibrium. The method based on Strang splitting is, once again, only first order.

	Strang Splitting	Quasi-Steady ($M = 2$)	Modified Flux Difference
dx	$\|p - p_0\|_1$	$\|p - p_0\|_1$	$\|p - p_0\|_1$
1.500×10^{-2}	5.553×10^{-4}	5.307×10^{-6}	5.881×10^{-6}
7.500×10^{-3}	2.775×10^{-4}	1.333×10^{-6}	1.483×10^{-6}
3.750×10^{-3}	1.390×10^{-4}	3.250×10^{-7}	3.775×10^{-7}
1.875×10^{-3}	6.970×10^{-5}	8.650×10^{-8}	1.386×10^{-7}
order	1.00	1.99	1.82

Four methods have been compared on this problem, a Strang-split method, the original quasi-steady method, a two-step quasi-steady method, and the method based on f-waves. Table 4.1 shows the one-norm errors generated by each method (the original quasi-steady errors are only included in Figure 4.5(a)). The table shows that both the quasi-steady method and the method based on f-waves generate second order solutions. The split method, however, is only first order on this problem. In addition, the split-method errors are a few orders of magnitude larger than those for the other two methods. Figure 4.5(a) shows a Log-Log plot of these errors. It is evident in this plot that both the quasi-steady methods, and the method based on f-waves do much better than the split method.

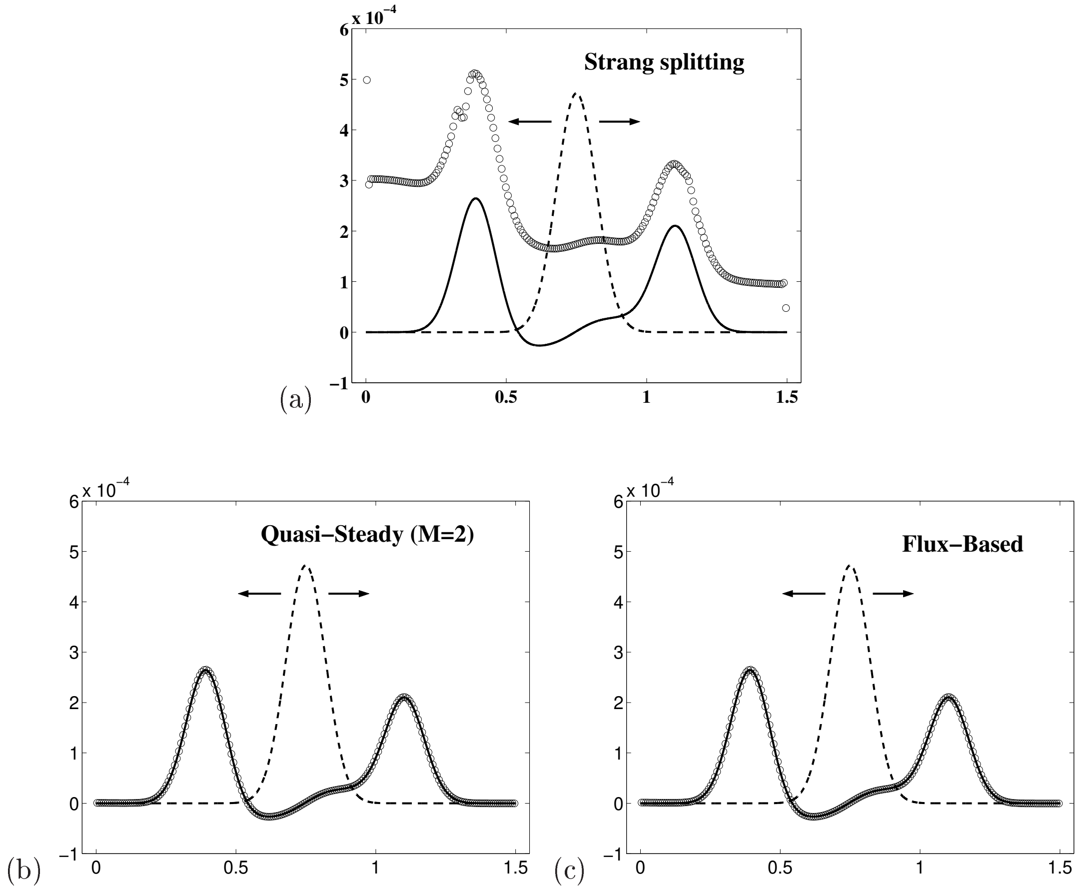

Figure 4.4: Numerical solutions for a smoothly perturbed isothermal Numerical results for the (a) Strang-split method, (b) quasi-steady method with $M = 2$, and (c) the method based on f-waves. Circles represent the computed values on a grid with 200 cells, the dashed line represents the initial condition, and the solid line was computed using the quasi-steady method on a grid with 8000 cells.

4.4 Perturbing the steady state

Now consider perturbing the equilibrium pressure field of the last section. We use a perturbed pressure defined by

$$p(t = 0, y) = p_0(y) + \epsilon \exp\left(-\frac{(y - y_0)^2}{\omega^2}\right), \tag{4.49}$$

where p_0 represents the equilibrium pressure and $0 < \epsilon \ll 1$. The resulting flow is essentially two acoustic pulses propagating away from this localized small disturbance. Figures 4.4(a) through 4.4(c) show the numerical results for pressure perturbation $p(t, y) - p_o(y)$ computed

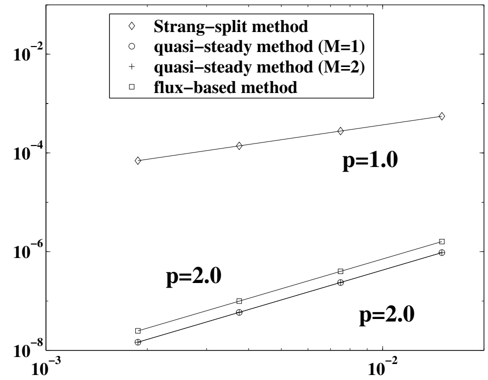

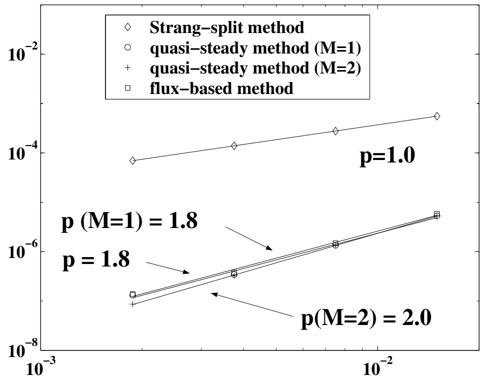

Figure 4.5: (a) Log-Log plot of the one-norm error in the perturbed pressure for the isothermal equilibrium. (b) Log-Log plot of the one-norm error for the perturbed equilibrium.

by the Strang-split method, a quasi-steady method with $M = 2$, and the method based on f-waves. Circles represent the computed values on a grid with 200 cells, the dashed line represents the initial condition, and the solid line was computed using the quasi-steady method on a grid with 8000 cells. The time was $t = 0.25$ when the computation was stopped. The pressure perturbation was set to $\epsilon = 4.76 \times 10^{-4}$.

Figure 4.4(a) demonstrates that when the perturbation is small enough, the split method fails to capture the correct value of the perturbed pressure. Notice that the split method has trouble maintaining the boundary values too. This is expected due to the fact that we are imposing boundary conditions on artificial problems equation (4.2) and equation (4.3). Both the quasi-steady method and the method based on f-waves, however, accurately capture the dynamics of the perturbation while maintaining the correct boundary values.

Table 4.2 shows the errors produced by each method. Once again, the two methods discussed in this chapter capture the dynamics to second order. The split method produces first order errors that are a few orders of magnitude larger than those produced by the other two methods. Figure 4.5(b) shows a Log-Log plot of these one-norm errors.

Typically, wave propagation methods are developed and applied to problems with discontinuities. It is important to know that the method is accurate in smooth regions of the solution, but it is equally important to know that discontinuities are sharply resolved. Figures 4.6(a) through 4.6(b) demonstrate that when the perturbation is discontinuous, it poses no problems for both methods discussed in this chapter. The split method fails to resolved the perturbation, or the boundary conditions.

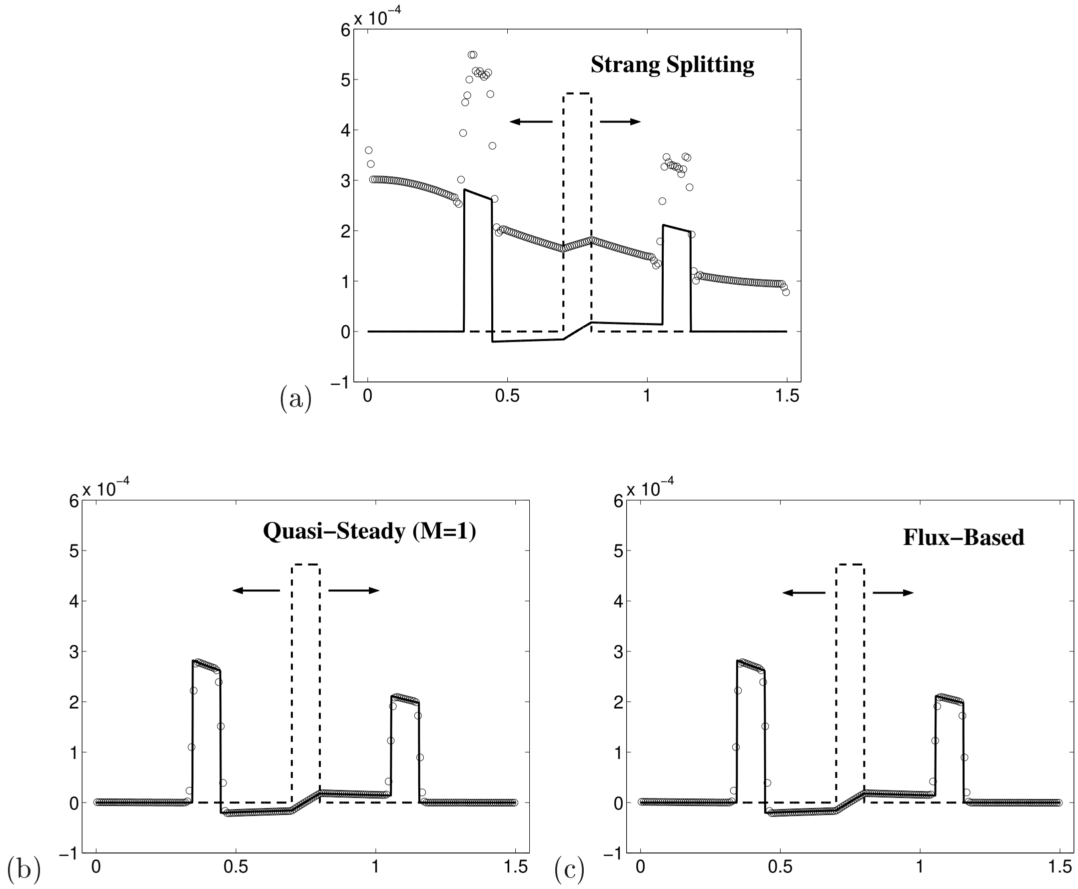

Figure 4.6: The same numerical methods are again applied to a perturbed isothermal equilibrium, but now the perturbation is not smooth. Both the quasi-steady method and the modified flux difference method handle the discontinuities very well.